H_2 Production by Zn Hydrolysis in a Hot-Wall Aerosol Reactor

Rodrigo J. Weiss, Hao C. Ly, Karsten Wegner, and Sotiris E. Pratsinis
Dept. of Mechanical and Process Engineering, ETH - Swiss Federal Institute of Technology, CH-8092 Zurich, Switzerland

Aldo Steinfeld
Dept. of Mechanical and Process Engineering, ETH - Swiss Federal Institute of Technology, CH-8092 Zurich, Switzerland, and Solar Technology Laboratory, Paul Scherrer Institute, CH-5232 Villigen, Switzerland

DOI 10.1002/aic.10437
Published online April 26, 2005 in Wiley InterScience (www.interscience.wiley.com).

A novel process for hydrogen generation from water at high conversion is presented that is based on zinc hydrolysis as part of the two-step water-splitting thermochemical cycle of Zn/ZnO redox reactions. It encompasses formation of Zn nanoparticles by steam-quenching a Zn(g) flow followed by in situ *hydrolysis. The process is experimentally demonstrated at the laboratory scale using a tubular aerosol flow reactor featuring a Zn-evaporation, a mixing and a reaction zone. In the reaction zone, operated at and just below the Zn(g) saturation temperature, Zn particles were formed and hydrolyzed with chemical conversion of up to 70%. The onset of H_2 formation is traced to ZnO formation by surface growth along the reactor axis using X-ray diffraction and microscopic analyses of Zn and ZnO particles collected on the reactor walls and effluents.* © 2005 American Institute of Chemical Engineers *AIChE J,* 51: 1966–1970, 2005

Introduction

Anthropogenic emissions of greenhouse gases and other pollutants can be significantly reduced or even completely eliminated by substituting fossil fuels by cleaner fuels, for example, solar hydrogen. Today, nearly all hydrogen is produced from fossil raw materials, mainly by steam reforming of natural gas. Several routes for the thermochemical production of hydrogen from water using solar energy have been examined.[1] Single-step thermal dissociation of water, although conceptually simple, has been impeded by the need of a high-temperature heat source for achieving a reasonable degree of dissociation, and by the need of an effective technique for separating H_2 and O_2 to avoid recombination. Water-splitting thermochemical cycles bypass the H_2/O_2 separation problem and further allow operating at relatively moderate upper temperatures. Thermodynamically efficient two-step water-splitting cycles, based on metal oxide redox reactions have been proposed.[2] The first, endothermic step is the solar thermal dissociation of the metal oxide to metal or lower-valence metal oxide. The second, nonsolar, exothermic step is the hydrolysis of the metal at moderate temperatures to form hydrogen and the corresponding metal oxide. Hydrogen and oxygen are formed in different steps, thereby eliminating the need for high-temperature gas separation. A number of metals (Mn, Zn, Fe, Ni, Co) have been proposed for this process. Of special interest is the solar thermochemical cycle based on ZnO/Zn redox reactions for its potential of achieving high energy conversion efficiency. The solar ZnO dissociation chemistry and the pertinent reactor technology are summarized by Steinfeld.[3]

This article focuses on the second step of solar H_2 synthesis by these reactions, Zn hydrolysis, which is thermodynamically favorable below 1,490 K. Clarke and Fray[4] investigated the oxidation of Zn vapor (made by H_2 reduction of ZnO pellets at high temperature) by hydrogen-water vapor mixtures in a silica flow reactor at 782 – 1123 K. They found that ZnO was formed on the tube walls by chemical vapor deposition making its efficient recovery difficult. Billings[5] reported the formation of ZnO by

Correspondence concerning this article should be addressed to S. E. Pratsinis at pratsinis@ptl.mavt.ethz.ch.

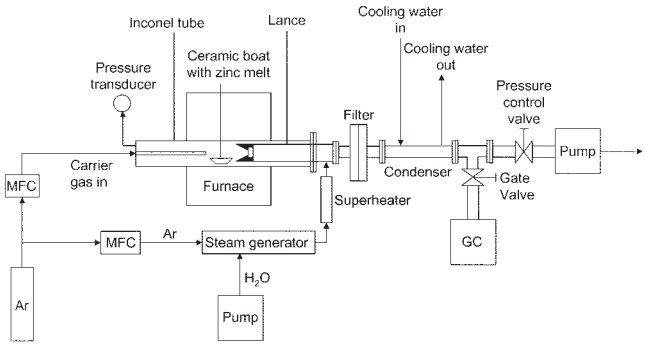

Figure 1. Aerosol reactor for H_2 synthesis by Zn hydrolysis.

oxidation of zinc vapor with steam at elevated temperatures during ZnO-char gasification. Weidenkaff et al.[6] studied the condensation of zinc vapor in the presence of O_2 by fractional crystallization in a temperature-gradient tube furnace and found that the oxidation of Zn is a heterogeneous process and, in the absence of nucleation sites, Zn(g) and O_2 can coexist in a meta-stable state. Hydrogen has been formed also by steam bubbling through molten zinc, resulting in 18 to 82% conversion of H_2O to H_2 at 723 to 773 K. The reaction rate, however, was inhibited by the formation of a ZnO(s) layer around the steam bubbles.[7]

The earlier studies have demonstrated the potential of the Zn/ZnO system for hydrogen generation, but the employed reactors have a number of shortcomings. An alternate process is the use of aerosol reactors for H_2 generation by Zn hydrolysis for their capacity to make high purity materials and to facilitate the subsequent gas-solid separation. One envisions formation of Zn nanoparticles by evaporation-condensation processes in which a Zn(g)-laden gas flow is quenched to reach over-saturation and, thus, condensation.[8,9,10] This can be followed or accompanied by *in situ* chemical reaction releasing H_2 and forming ZnO as in AlN synthesis by ammonolysis of Al in an aerosol flow reactor.[11] In fact, in the latter study, H_2 had been inadvertently produced in a hot-wall reactor without reporting it.

Here, bulk Zn metal is heated in a hot-wall aerosol reactor forming Zn-laden gases that are cooled and hydrolyzed by steam as they exit the reactor. The effect of process parameters on product characteristics and H_2 conversion efficiency is investigated by X-ray diffraction, electron microscopy and gas chromatography. Emphasis is placed on understanding the Zn/ZnO solid composition which is directly related to H_2 conversion as a function of temperature along the reactor axis. The advantages of such a combined process are the simple, continuous and controllable feeding of reactants and removal of products and the enhanced conversion by the high specific surface area of Zn nanoparticles.

Experimental

The experimental setup is shown in Figure 1.[12] The reactor is made by an Inconel tube (100 cm length, 5.25 cm i.d.) with its middle section placed into a tube furnace (Carbolite CFM 14/1, 30 cm-heated length) to evaporate Zn (Riedel-de Häen, 99.99%) from an alumina crucible (Alsint 99.7%). Argon carrier gas (Pan Gas, 99.999%) controlled by a mass flowmeter (Bronkhorst EL-Flow 201 A) is introduced through a 0.22 cm i.d. Inconel tube and discharged above the crucible. The inlet tube is supported by a stainless steel flange that contains a pressure transducer (MKS PDR2000) and closes the feed side of the reactor.

The reactor end flange concentrically holds a stainless steel lance, consisting of a 1.65 cm i.d. center tube. The lance is positioned inside the tubular reactor 8 cm after the ceramic crucible and serves as the mixing and reaction zone (Figure 2). Superheated steam diluted in Ar is introduced into the reactor in a counterflow to the Zn-laden carrier gas through an array of 12 equally-sized nozzles of 2.5 mm i.d. uniformly arranged at the front side of the lance. A stainless steel gas return cap, as shown in Figure 2, is mounted on the lance to guide the steam perpendicularly to the Zn-laden carrier gas stream, thus forming a T-mixer. Products, reactants and Ar gas exit the reaction zone through the center tube of the lance with the aid of a vacuum pump (Vacuubrand, RZ 16). The steam is provided by an external generator with a peristaltic pump (Ismatec MCP-552). Prior to entering the lance, the steam is superheated to 623 K.

The reactor outlet is connected to a glass fiber filter (Whatman GF/A, diam. 150 mm) on a stainless steel filter holder for particle collection. Excess water is removed from the product gas mixture (Ar, steam, and H_2) by a condenser behind the filter. All tube connections are made gas-tight with vacuum flanges (Balzers KF-series). The reactor pressure is controlled by a butterfly valve (MKS 653B) in front of the vacuum pump (Figure 1). The effluent gas composition is analyzed by a gas chromatograph (GC, MTI, Analytical Instruments P200) connected with a gate valve behind the condenser.

The temperature profile of the reaction zone was measured ($\pm$ 10 K) in the absence of Zn and steam by a 1 mm K-type thermocouple along the lance centerline. As the inner diameter of the outlet tube is only 1.6 cm, it is reasonable to assume that the wall temperature does not significantly vary from the centerline temperature.[12] The change in the temperature by the released heat from the exothermal hydrolysis reaction is negligible as rather dilute aerosols were employed here (for example, compare the hydrolysis energy corresponding to a power of 6 W for the conditions at 1,073 K and 0.5 W at 923 K to the furnace power of 2.8 kW). Particle wall deposits were examined on a stainless steel rod (39 cm long, 1 cm wide and 2 mm thick) placed into the center tube of the lance. After the experiments, the rod was divided into three equal sections of 13 cm each, and the deposits were scraped off for XRD analysis.

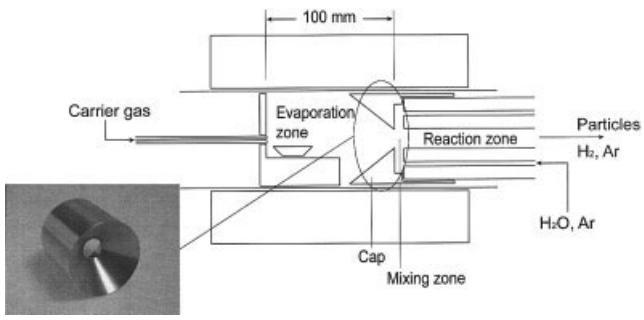

Figure 2. Reactor configuration with picture inset of the cap separating the Zn evaporation zone from the mixing and reaction zones.

This is similar to Kim[13] who quantitatively determined the particle deposition rate to the aerosol reactor walls at high temperatures. Product powders were analyzed by X-ray diffraction (XRD, Bruker D8 Advance, Cu K_α-radiation). The crystallite size and phase composition of the wall (rod) deposits and product powders were obtained by XRD using the Rietveld method and the fundamental parameter approach.[14]

Prior to each experiment, the crucible loaded with weighed zinc pellets was placed in the evaporation zone of the reactor (Figure 2). The reactor was closed, evacuated to 25 mbar, and subsequently purged with Ar to 1250 mbar with the gate valve remaining closed throughout the evacuation and purging process. This procedure was repeated three times until the amount of O_2 detected by the GC remained at a constant level of 0.3 – 0.4%. It was not possible to obtain a complete oxygen free system, as the reactor was not fully gas-tight at subatmospheric pressure. During a typical experimental run, the reactor was heated at 20 K/min to the desired temperature without any gas flow. Once the desired temperature was attained, the carrier gas over the Zn melt was turned on, followed by the steam-Ar flow. The carrier gas had to be switched on first to prevent steam backflow into the evaporation zone that would oxidize the zinc melt. After each experiment, the argon and steam flows were switched off, and air was introduced into the reactor to oxidize the zinc melt surface, thus stopping the evaporation. Each experiment lasted 15–20 min. The crucible was weighed to determine the amount of evaporated zinc.

The influence of the furnace temperature on H_2 conversion was investigated for various H_2O:Zn molar ratios that were controlled by the water feed rate through the peristaltic pump in the range of 2.3 – 33.2 g/h giving excess steam at all conditions. All experiments were carried out at 923, 1,023, and 1,073 K furnace set temperature, with 0.5 and 1.5 L/min Ar carrier gas (Zn) and dilution gas (steam), respectively, reported at normal conditions (273 K and 1 bar). Hydrogen was formed by H_2O (steam) decomposition on Zn forming ZnO and H_2. Here all experiments were carried out in excess of water, while other studies were carried out in excess of Zn as with Berman and Epstein.[7] The H_2 conversion is determined with respect to the limiting reactant of that reaction

$$\text{Conversion}\,[\%] = \frac{\text{moles of } H_{2,\text{GC}}}{\text{moles of } H_{2,\text{max}}}$$

where $H_{2,GC}$ refers to H_2 measured by GC, and $H_{2,max}$ to the theoretical maximum amount of H_2 that could have been produced under complete hydrolysis of the evaporated zinc. It should be noted that thermodynamic calculations give maximum conversion of 99.6%, 98.4% and 97.0% for 923 K, 1,023 K and 1,073 K, respectively. Using these values, the reactor performance (conversion) would increase slightly. Assuming complete hydrolysis, results in conservative values for the H_2 conversion while facilitating the calculations.

Results and Discussion

Figure 3 shows the average conversion to H_2 (triangles), and the evaporation rate of Zn (circles) along with the theoretical one (solid line) as a function of the evaporation zone set temperature. The theoretical evaporation rate was determined by the Zn partial pressure that was calculated with Antoine's equation and assuming full saturation of the Ar carrier gas. The bars at the data points indicate the range of the variable at multiple runs (Zn evaporation) or at different H_2O:Zn ratios (H_2 conversion). Increasing the temperature naturally increases the evaporation rate of Zn. The Zn-laden Ar carrier gas, however, is not saturated as the residence time of the carrier gas is not sufficient for saturation in these reactors, for example, as observed in Al evaporation.[15]

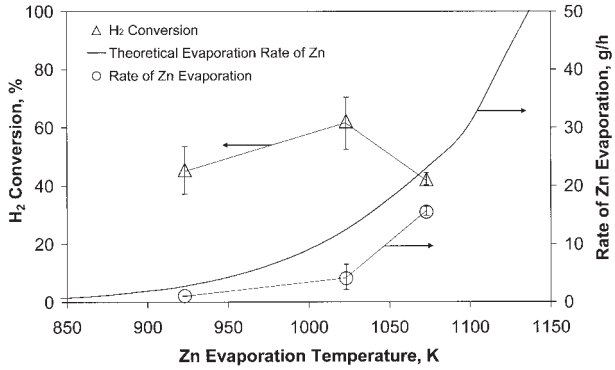

Figure 3. Zinc evaporation rate (circles) and H_2 conversion efficiency of H_2O (triangles) with respect to the limiting reactant (here Zn) as a function of Zn evaporation temperature.

The solid line is the evaporation rate assuming 100% saturation of the carrier gas.

The H_2 conversion ranges from 37 to 72% at 923 and 1,023 K, respectively, while the average conversion increases from 45% at 923 to 60% at 1,023 K and decreases again to 37% at 1,073 K. The H_2 concentration in the off-gas was 0.13, 0.71, and 1.87 vol % at 923, 1,023, and 1,073 K, respectively. Low evaporation temperatures favor low Zn evaporation rates, which in turn leads to the formation of fine Zn particles with high specific surface area upon cooling in the mixing and reaction zones as with AlN[11] and Bi.[12] Increasing T increases Zn particle concentration and size that promote higher H_2 conversions with respect to fed-Zn that seem, however, to reach an optimum at 1,023 K. At higher T, the H_2 conversion decreases as larger Zn particles of lower specific surface areas are formed analogous to the synthesis of Al particles in these reactors.[15] The measured H_2 conversion was not affected significantly (1 – 5%) by the water vapor pressure, which is consistent with Clarke and Fray[4] who only observed such a dependence above 1,073 K. In addition, these H_2 conversions with respect to the limiting reactant (here Zn) were comparable to those measured in molten Zn, 17 – 83% with respect to the limiting reactant (there fed-H_2O), although there the conversion decreased with increasing water vapor pressure.[7]

At all conditions, XRD-pure Zn particles were collected on the reactor outlet filter. A thin passivating oxide layer that forms on metal surfaces when exposed to oxygen was not detectable by XRD as with Bi nanoparticles.[12] The phase composition of the particles deposited on the reaction zone walls (inside the inner tube of the lance) at 1,073 K evaporation zone set temperature, 0.5 L/min Ar carrier gas and 7.7 g/h water flow was determined by XRD. Figure 4 shows the temperature profile along the reaction zone axis and the location of the various sampling rod sections along with that of the

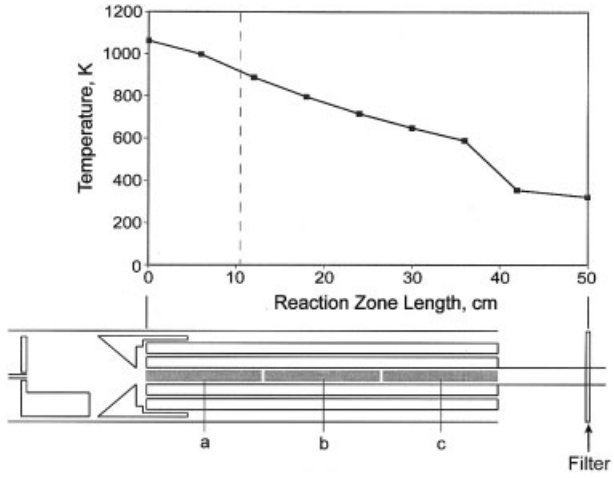

Figure 4. Centerline temperature and the three sampling sections: the dashed line at 11 cm shows the point where saturation is reached.

filter. The dashed region shows the section of the reactor above the Zn saturation temperature for the actual Zn-concentration in the reaction zone that corresponds to 910 K. In this region, neither Zn particles are expected to be formed by condensation nor ZnO particles by Zn vapor hydrolysis in the gas phase, as corroborated by XRD analysis of deposits.

The reactor wall deposits were examined by XRD analysis on the rod that was divided into three sections of 13 cm each. Figure 5 shows the XRD spectra of each rod section and filter, while Figure 6 shows the corresponding mass fraction of ZnO (circles) as well as the XRD average crystal size of ZnO (squares) and Zn (triangles). The deposits on the first section of the rod, closest to the evaporation and mixing zones, show the characteristic sharp ZnO peaks of a wurtzite or zincite structure. The deposits on the corresponding reaction zone walls were identical, at least in appearance, and formed a hard grayish film. A typical TEM picture of these deposits is shown in Figure 7 (section a). There, the crystals are well structured with average XRD size of 93 nm. Hardly any aerosol particles have been formed in this section as most of it is above the saturation temperature of Zn (Figure 4). As a result, the observed ZnO deposits must form by a surface reaction of Zn(g) and steam consistent with Clarke and Fray[4] and Weidenkaff et al.[6]. The complete absence of Zn metal there further supports a surface reaction mechanism.

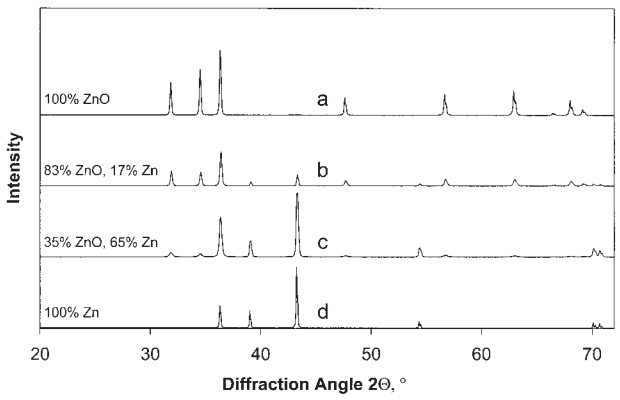

Figure 5. XRD patterns of the deposits collected in the first (a), middle (b), and last (c) section, as well as on the filter (d).

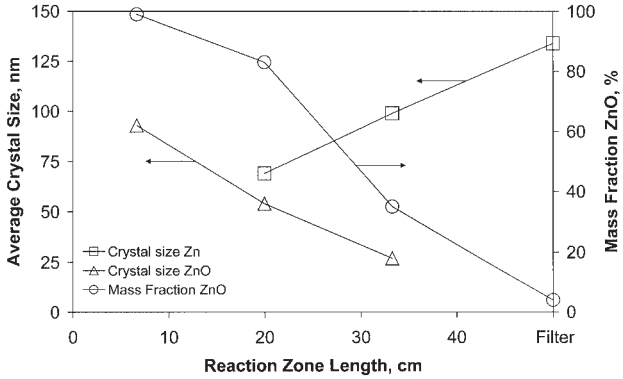

Figure 6. ZnO mass fraction (circles) and the corresponding Zn (squares) and ZnO (triangles) average XRD crystallite size of the deposits on the reactor walls and on the filter.

In the middle of the rod (section (b)), a grainy, grayish deposit is formed consisting of 17 and 83 wt %, Zn and ZnO, respectively (Figure 5 and 6). The crystallite sizes are comparable, 69 and 54 nm for Zn and ZnO, respectively. The morphology of these deposits is dramatically different than those of the previous section (Figure 7, section (b)). Filamentary, polycrystalline structures several μm long and about 100 nm thick may indicate initial Zn particle formation by condensation followed by deposition on the reactor walls and subsequent ZnO formation on the surface of these immobilized particles for the duration of the experiment. Micro- and even nanorods of ZnO have been grown by vapor deposition processes at similar temperatures.[16]

In section (c) further downstream and closer to the filter, the deposits look similar but with thicker filaments (Figure 7, section

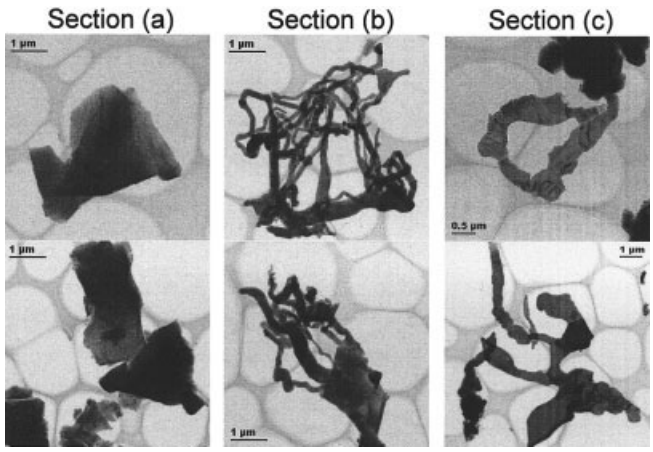

Figure 7. TEM pictures of the deposits on the walls at the three sections along the reaction zone.

The layer-like pure ZnO deposit of section (a) was built up by chemical vapor deposition while the powders collected in section (b) and (c) are made from filamentary particles containing both Zn and ZnO crystallites.

c) than those of section (b) while there the Zn crystallites (65 wt %) are significantly larger (about 100 nm) than those of ZnO (about 20 nm and 35 wt %). The large difference in size and the close one in mass composition indicate further a Zn core covered by a ZnO layer structure rather than separate Zn and ZnO particles. It is plausible that longer gas-phase residence times of particles deposited in section (c) lead to larger Zn particles than in section (b). On the surface of these immobilized Zn particles in both sections, ZnO grows by surface reaction.[4] The lower temperature of section (c) slows down the growth of ZnO crystallites. As on the filter, only Zn particles of 130 nm crystallite size were collected indicating further that Zn particles grew in the gas phase by condensation and/or coagulation beyond that of particles collected on section (c). Again, this is consistent with Clarke and Fray[4] who observed that on the walls of their flow reactor the ZnO film thickness decreased with decreasing temperature along the reactor axis until it vanished, and then a mirror coating of Zn had been formed that had condensed from the gas at temperatures below the Zn dewpoint. It should be noted that the deposits of section (a) adhered stronger to the reactor walls than those at section (b) and (c). The higher temperature and the dominance of surface reaction in section (a) could have contributed to stronger adhesion between the particles and reactor walls.

The residence time in the gas phase was probably too short, and the temperature on the filter was too low for ZnO formation and subsequent H_2 production. This is consistent with AlN formation by nitridation of Al with N_2 gas in aerosol reactors where XRD-pure Al was collected on the filter while AlN was found on the reactor walls. In contrast, when excess N_2 and adequate residence times were allowed, AlN particles were collected on the filter as well.[11]

It is expected that the chemical conversion is hindered by the formation of a passivating layer of ZnO or $Zn(OH)_2$ at lower temperatures. Thus, the diffusion of steam through this oxide layer becomes the predominant rate limiting mechanism. Furthermore, the lower temperatures further downstream result in slower hydrolysis kinetics and, consequently, lower chemical conversions. The Zn crystal growth along the reaction axis and the simultaneous decrease in size of the ZnO crystals (Figure 6) could be an indication that the specific surface area of the Zn nanoparticles also increases as the particles move further downstream. This may imply that the optimal temperature for the combined nanoparticle formation and *in situ* hydrolysis is just below the Zn(g) saturation temperature.

Summary and Conclusions

A novel approach for generation of hydrogen by hydrolysis of Zn nanoparticles was developed, in which Zn-vapor is quenched with steam, forming Zn-nanoparticles that are hydrolyzed *in situ* to generate ZnO and H_2. This Zn-hydrolysis reaction is part of a 2-step water-splitting thermochemical cycle using concentrated solar power. The conversion efficiency to H_2 with respect to the limiting reactant (here Zn) is 37 – 72% that is comparable to existing solar hydrogen processes. This combined process offers high specific reaction area for a high degree of chemical conversion. It should be mentioned, however, that the H_2 concentration of 0.13% to 1.87% in the outlet gas stream will have to be increased for an efficient recovery and, thus, commercialization.

The proposed combined process was experimentally demonstrated at the laboratory scale using a tubular aerosol flow reactor featuring distinct zones for Zn evaporation, nanoparticle formation by mixing and steam quenching, and *in situ* hydrolysis and H_2 production. Zn nanoparticles were formed by nucleation and grew by condensation and coagulation, while ZnO crystallites grew by surface reaction on the newly formed but immobilized particles resulting in filamentary deposits on the reactor walls. The degree of ZnO and, subsequently, H_2 conversion decreased with temperature, presumably as a result of the formation of a ZnO passivating layer on larger particles. This undesired reaction barrier can be minimized by controlling the reactor temperature and reducing the size of Zn nanoparticles.

Acknowledgments

This project was jointly funded by the BFE-Swiss Federal Office of Energy and the Swiss Commission of Technology and Innovation (Top-Nano21 grant No. 6740.1 TNS).

Literature Cited

1. Steinfeld A. Solar Thermochemical Production of Hydrogen - A Review. Solar Energy. 2005;78:603–615.
2. Steinfeld A, Kuhn P, Reller A, Palumbo R, Murray J, Tamaura Y. Solar-processed metals as clean energy carriers and water-splitters. *Int J Hydrogen Energy*. 1998;23:767-774.
3. Steinfeld A. Solar hydrogen production via a two-step water-splitting thermochemical cycle based on Zn/ZnO redox reactions. *Int J Hydrogen Energy*. 2002;27:611-619.
4. Clarke JA, Fray DJ. Oxidation of zinc vapour by hydrogen-water vapour mixtures. *Trans Inst Min Metall*. 1979;C 88:C161–C166.
5. Billings WG. Zinc Oxide-Char Gasification Process. U. S. Patent 4,496,370 1985.
6. Weidenkaff A, Steinfeld A, Wokaun A, Eichler B, Reller A. The direct solar thermal dissociation of ZnO: Condensation and crystallization of Zn in the presence of oxygen. *Solar Energy*. 1999;65:59-69.
7. Berman A, Epstein M. The kinetics of hydrogen production in the oxidation of liquid zinc with water vapor. *Int J Hydrogen Energy*. 2000;25:957-967.
8. Kimoto K, Kamiya Y, Nonoyama M, Uyeda R. An electron microscope study on fine metal particles prepared by evaporation in argon gas at low pressure. *Jap J Appl Phys*. 1963;2:702-713.
9. Buckle ER, Pointon KC. Condensation of zinc aerosols. *J Mater Sci*. 1977;12:75-89.
10. Daub O, Langel W, Reiner C, Kienle L. QMS-Controlled production of nanocrystalline metals by inert gas condensation in a flow system. *Ber Bunsenges Phys Chem*. 1997;101:1753-1756.
11. Pratsinis SE, Wang G, Panda S, Weimer AW, Guiton T. Aerosol synthesis of AlN by nitridation of aluminum vapor and clusters. *J Mater Res*. 1995;10:512-520.
12. Wegner K, Walker B, Tsantilis S, Pratsinis SE. Design of metal nanoparticle synthesis by vapor flow condensation. *Chem Eng Sci*. 2002;57:1753-1762.
13. Kim KS. Analysis on SiO_2 particle generation and deposition using tube furnace reactor. *AIChE J*. 1997;43:2679-2687.
14. Cheary RW, Coelho AW. A fundamental parameter approach to x-ray line-profile fitting. *Appl Crystallogr*. 1992;25,109-121.
15. Panda S, Pratsinis SE. Modeling the synthesis aluminum particles by evaporation-condensation in an aerosol flow reactor. *Nanostructured Mater*. 1995;5:755-767.
16. Zhao QX, Willander M, Moran RE, Hu QH, Campbell EEB. Optical recombination of ZnO nanowires grown on sapphire and Si substrates. *Appl Phys Lett*. 2003;83:165-167.

Manuscript received July 6, 2004, and revision received Oct. 27, 2004.